

ExoMol line lists VII: The rotation-vibration spectrum of phosphine up to 1500 K

Clara Sousa-Silva, Ahmed F. Al-Refaie, Jonathan Tennyson and Sergei N. Yurchenko
Department of Physics and Astronomy, University College London, London WC1E 6BT, UK

Accepted XXXX. Received XXXX; in original form XXXX

ABSTRACT

A comprehensive hot line list is calculated for $^{31}\text{PH}_3$ in its ground electronic state. This line list, called SALTY, contains almost 16.8 billion transitions between 7.5 million energy levels and it is suitable for simulating spectra up to temperatures of 1500 K. It covers wavelengths longer than $1\ \mu\text{m}$ and includes all transitions to upper states with energies below $hc \cdot 18\,000\ \text{cm}^{-1}$ and rotational excitation up to $J = 46$. The line list is computed by variational solution of the Schrödinger equation for the rotation-vibration motion employing the nuclear-motion program TROVE. A previously reported *ab initio* dipole moment surface is used as well as an updated ‘spectroscopic’ potential energy surface (PES), obtained by refining an existing *ab initio* surface through least-squares fitting to the experimentally derived energies. Detailed comparisons with other available sources of phosphine transitions confirms SALTY’s accuracy and illustrates the incompleteness of previous experimental and theoretical compilations for temperatures above 300 K. Atmospheric models are expected to severely underestimate the abundance of phosphine in disequilibrium environments, and it is predicted that phosphine will be detectable in the upper troposphere of many substellar objects. This list is suitable for modelling atmospheres of many astrophysical environments, namely carbon stars, Y dwarfs, T dwarfs, hot Jupiters and solar system gas giant planets. It is available in full as supplementary data to the article and at www.exomol.com.

Key words: molecular data; opacity; astronomical data bases: miscellaneous; planets and satellites: atmospheres; stars: low-mass; stars: brown dwarfs.

1 INTRODUCTION

Over the past twenty years, discoveries of planets, stars and substellar objects have demonstrated the enormous diversity of astrophysical bodies in the Universe. Thanks to modern techniques and technology, it is now possible to study the atmospheres of these objects and retrieve some knowledge of their composition, structure and dynamics. However, these are extremely complex systems to model and accurate observations are still difficult to perform. In particular, it is

crucial for the correct characterisation of these atmospheres that complete and accurate descriptions of the molecules that comprise them are available. Here phosphine, or PH_3 , is considered.

Phosphorus is the one of the most abundant chemically reactive volatile elements in a solar type system (with S, after H, C, N and O). Although phosphorus has considerably smaller cosmic abundances than H, O, C or N, it is predicted to have an important role in atmospheric chemistry and dynamics. Phosphorus is not particularly common in the universe but it is ubiquitous and is important for most essential biochemical functions. Due to its role as biogenic particle, phosphorus could potentially be used in the search for extinct or extant life in other planets (Maciá 2005).

A large fraction of the existing phosphorus in various astronomical environments is expected to be found in the form of phosphine, or PH_3 (Agundez et al. 2014; Visscher et al. 2006). Phosphine is an extremely toxic, semi-rigid, relatively stable, oblate, symmetric-top molecule, and has so far been detected in the lower troposphere of the Earth, the atmospheres of Jupiter and Saturn, and in the carbon star envelope IRC +10216 (Prinn & Lewis 1975; Edgington et al. 1998; Fletcher et al. 2009; Agundez et al. 2014; Tarrago et al. 1992).

Partially due to the lack of strong absorption from CH_4 , the $5\ \mu\text{m}$ spectral window is a region of low opacity in Jupiter, Saturn and the Earth's atmosphere. Alongside other molecules (CO , GeH_4 , AsH_3), PH_3 is partly responsible for the continuum opacity in this region and has detectable absorption bands (Noll & Marley 1997a), specifically the $2\nu_2$ overtone bending band. In Jupiter, phosphorus is found at approximately tropospheric solar abundances (1.1 ppm) in the form of phosphine, and is over four times more abundant in Saturn (4.5 ppm), also as phosphine (Noll & Marley 1997a; Owen & Encrenaz 2003; Moreno et al. 2009; Visscher et al. 2006). This agrees with models of core accretion that expect Saturn to have a considerably larger fraction of ice to gas than Jupiter. In both planets, this abundance of a disequilibrium species like phosphine at observable levels of the atmosphere reflects both a large reservoir in deep regions of the planets and the strength of the convective transport of the molecule.

In local thermochemical equilibrium (LTE), P_4O_6 would be expected to dominate the upper atmospheres of planets with approximate solar abundances. However, almost no P_4O_6 is found in these environments because phosphine quenching and rapid vertical mixing from regions where PH_3 is dominant leads to high disequilibrium abundances. This quenching occurs because timescales for the conversion of PH_3 to P_4O_6 are much larger than the convective timescales, so the production of P_4O_6 is kinetically inhibited (Moses 2014; Visscher et al. 2006; Fegley Jr & Lodders 1996). Disequilibrium chemistry is expected to lead to phosphine being orders of magnitude more abundant than predicted by equilibrium models, both for environments where $T \geq 2000\text{ K}$ and at the uppermost atmosphere of most substellar objects (Moses 2014).

The thermal decomposition of phosphine at high temperatures has been studied for a long time, starting with Hinchelwood & Topley (1924). Recently Visscher et al. (2006) discussed at length the pressure and temperature parameters at which phosphine is expected to be found in solar composition and LTE environments. At 1 bar, phosphine is predicted to be a dominant phosphorus carrying molecule in environments with temperatures up to about 1500 K, and it is expected to contribute to the composition of atmospheres up to about 2500 K if the pressure is above 3 bar.

The detection of phosphine can therefore be used as a chemical probe for deep layers of both Jupiter and Saturn's atmosphere, as it is only present at the top layers through vertical mixing. Analysis of future observations of Jupiter from NASA's TEXES, NASA's Juno and ESA's JUICE will require accurate data on phosphine, and past observations of Saturn from Cassini/VIMS and Cassini/CIRS will gain from further understanding its spectrum (Encrenaz et al. 2014; Fletcher et al. 2009). Suspected inaccuracies found in regions of the existing phosphine data may be behind misinterpretation of previous astronomical data (Malathy Devi et al. 2014). Additionally, JUNO will cover the full latitude and longitude of Jupiter and its analysis of the polar atmosphere of Jupiter should confirm a depletion of phosphine in the polar vortices analogous to Saturn's (Fletcher et al. 2009). Titan has also been predicted to contain phosphine, but spectrum recorded with Cassini CIRS failed to detect any, putting an upper limit of 1 ppb on the phosphine abundance of its atmosphere (Nixon et al. 2013). Similar unsuccessful detections of phosphine in Neptune and

Uranus suggest that the abundance of phosphorus on these planets is sub solar (Moreno et al. 2009), with an upper limit of 0.1 times solar P/H abundance.

The existence of phosphine outside the Solar System has recently been confirmed by Agundez et al. (2014) in the carbon star envelope IRC +10216, with an abundance of 10^{-8} relative to H_2 . This was done using the HIFI instrument on board Herschel. Together with HCP, PH_3 is one of the major phosphorus carriers in the inner circumstellar regions.

There have been multiple predictions of phosphine in many other astrophysical environments, but its presence and formation scenarios remain poorly understood and none has been found outside the solar system other than the aforementioned discovery of circumstellar phosphine in IRC +10216. This is due to a variety of factors, including the sparsity of fundamental data which this work is rectifying. Below are some of the expectations for further phosphine detection.

A particular region of interest is the 4.1-5.1 μm window, which is found to be an interval of very low opacities in both Jupiter and Saturn. It is therefore expected that detection of PH_3 in this region could be used as a marker for vertical convection and a tracer for tropospheric dynamics in the upper atmospheres of other astronomical bodies, namely Hot Jupiters and Brown Dwarfs.

In Y dwarfs, with $T_{\text{eff}} \approx 500$ K, phosphine should exhibit a strong feature in the mid-infrared at 4.3 μm (Morley et al. 2014), where it is predicted to be the dominant source of opacity. T dwarfs, with $T_{\text{eff}} \leq 1300$ K, will mostly be dominated by other molecules (e.g. H_2 , NH_3 , CH_4 , CO , H_2O and CO_2) but phosphine can still have a significant contribution to the shape of the spectrum. The NIRSpect near-infrared spectrograph on JWST will be able to collect spectra in the 2.9-5 μm region with sufficient sensitivity to detect the presence or absence of phosphine, particularly for slightly cooler Y dwarfs with $T_{\text{eff}} \leq 450$ K (Morley et al. 2014).

Phosphine is predicted to be the dominant phosphorus molecule in cool T dwarfs like Gliese 229B where it is expected to carry all the phosphorus in the atmosphere to the top layers, with approximately 0.6 ppm. PH_3 should be detectable (for resolutions higher than 1.2 cm^{-1}) in the 4.45-5.40 μm spectral window of Gliese 229B, particularly the 4.3 μm feature (Noll & Marley 1997a; Fegley Jr & Lodders 1996). Models estimate that, for regions where $T \geq 1155$ K, the major phosphorus carrying gas in Gliese 229B is phosphine, with rapid vertical mixing quenching its destruction (Fegley Jr & Lodders 1996). As the temperature rises, PH_3 is converted to P_4O_6 , but it should still be present at observable heights.

In hotter environments, like HD209458b and L dwarfs, where phosphorus equilibrium chemistry is approached, the phosphine abundances decrease significantly to about 50 ppb (Visscher et al. 2006). It is still possible to detect phosphine in these atmospheres, but higher resolution is required to distinguish its features from that of neighbouring CO bands (Noll & Marley 1997a). However, phosphine is expected to be the dominant phosphorus carrying species at the observable atmosphere of hot T dwarfs and cool L dwarfs, with effective temperatures between 1000 and 1400 K (Visscher et al. 2006).

There are still disequilibrium effects that are not completely understood. For example, observations of Saturn's upper troposphere found that phosphine abundances decreased with depth (Malathy Devi et al. 2014), contradicting the proposal that phosphine is dredged up through vertical mixing from deeper layers of the atmosphere. This depletion is not understood, as there is no known formation mechanism for phosphine at the upper levels of Saturn's atmosphere that could lead to the abundances observed. Suggested explanations for this inconsistency are a poor understanding of the aerosol opacity in the VIMS observations and intensity uncertainties in the molecular data.

Future detections of phosphine can only be achieved by accurately modelling these atmospheres. This requires an extensive knowledge of the temperature dependent spectrum of phosphine, which can only be established with a comprehensive line list.

There are multiple sources of phosphine data (Müller 2013; Kshirsagar 2007; Temma et al. 2006; Cazzoli & Puzzarini 2006; Butler et al. 2006; Wang et al. 2005; Ulenikov et al. 2004; Salem et al. 2004; Ulenikov et al. 2002; Suarez 2002; Brown et al. 2002; He et al. 2001; Fusina & Di Lonardo 2000; Ainetshian et al. 1997; Tarrago et al. 1992, 1981; Pickett

et al. 1981; Belov et al. 1981; Baldacci et al. 1980; Helms & Gordy 1977; Chu & Oka 1974; Davies et al. 1971; Helminger & Gordy 1969; Loomis & Strandberg 1951; Wang et al. 2000; He et al. 2001; Yurchenko et al. 2003, 2005b, 2006; Ovsyannikov et al. 2008a,b; Nikitin et al. 2009), both experimental and theoretical, which are further described in our previous paper on room temperature phosphine (Sousa-Silva et al. 2013). Additionally, a recent paper by Malathy Devi et al. (2014) improved the experimental phosphine spectrum for the 4.08–5.13 μm region, which, as mentioned above, is of particular importance due to it being an interval of low opacity in gas giants and brown dwarfs (Noll & Marley 1997b). Most of these experimental sources have already been incorporated in the HITRAN database (Rothman et al. 2013) and collectively contain less than 30 000 lines, and no wavelength coverage shorter than 2.7 μm .

Despite these efforts, no complete line list for hot phosphine exists in the literature. The line lists mentioned above only cover low values of rotational excitations, a small number of bands, and some regions are missing altogether. Often, contamination of gas samples affects the measured intensities (Malathy Devi et al. 2014), and this can be an effect that is hard to accurately compensate for. It is not unusual for experimental data with extremely accurate line positions to have intensity uncertainties well above 10%. Additionally, all the experimental datasets mentioned above are designed to be used only at room temperature and below. Consequently, they are insufficiently complete to be appropriate for use in the characterisation of atmospheres of any astronomical bodies at higher temperatures.

A theoretical line list for phosphine was previously computed by us (Sousa-Silva et al. 2013), henceforth SYT. However, although SYT contains many orders of magnitude more lines than any previous phosphine line list (137 million transitions between 5.6 million energy levels), it too was only designed to be accurate for temperatures below 300 K, making it unsuitable for most astronomical studies. Since HITEMP (Rothman et al. 2010), HITRAN’s high-temperature database, does not include phosphine, SAIKY is the first line list suitable for modelling phosphine spectra in environments up to 1500 K. The completeness and coverage of the SAIKY line list makes it particularly suitable for studies of non-LTE environments.

The current work is performed as part of the ExoMol project. This project aims to provide line lists of spectroscopic transitions for key molecular species which are likely to be important in the atmospheres of extrasolar planets and cool stars; its aims, scope and methodology are summarised in Tennyson & Yurchenko (2012). The SAIKY line list builds on previously released ones for polyatomic hydrides such as water (Barber et al. 2006), ammonia (Yurchenko et al. 2011), formaldehyde (Al-Rafaie et al. 2014), and methane (Yurchenko & Tennyson 2014; Yurchenko et al. 2014). Finally we note that energy levels generated for this work have been used as part of a study to compute thermodynamic properties of phosphine and ammonia, including its partition function, for temperatures up to 6000 K (Sousa-Silva et al. 2014).

2 OVERVIEW OF THE SAIKY LINE LIST

In the following PH_3 and phosphine will refer to the main isotopologue $^{31}\text{PH}_3$, since ^{31}P is the only non-synthetic, stable isotope of phosphorus.

SAIKY is a catalogue of transitions, each characterised by a frequency, its lower and upper energy level, Einstein coefficient and quantum numbers. Together these fully describe the spectrum of the phosphine molecule within the frequency range 0 – 10 000 cm^{-1} , or wavelengths longer than 1 μm . It contains 16 803 703 395 transitions between 7 480 690 energy levels below 18 000 cm^{-1} , with rotational quantum number J values up to 46. The highest energy state considered is 18 000 cm^{-1} above the zero-point energy (5 213.9280 cm^{-1}) for phosphine, as the intensity of transitions to higher energy levels is too weak to be important, even at temperatures of 1500 K. Consequently, to ensure that the line list is complete within the frequency range 0 – 10 000 cm^{-1} , the highest lower energy state considered is 8 000 cm^{-1} . All transitions are within the ground electronic state of phosphine, since the first excited electronic state is above the dissociation limit of the molecule.

The strongest SAIKY transition has an Einstein- A coefficient of 89.1 s^{-1} while the weakest lines go down to 10^{-48}

s^{-1} . In non-LTE environments even extremely weak lines can play an important role in the shape of a spectrum. This is the reason behind including transitions with extremely weak absorptions in SAITY.

The final line list is presented in the ExoMol format (Tennyson et al. 2013), with a transition file ordered in increasing transition frequency and an energy file. The former contains a description of each transition by its upper (final) and lower (initial) energy level reference numbers (f and i), as well as the electric dipole transition probability represented as an Einstein coefficient A_{if} in s^{-1} . Using this information, the line intensity of each transition can be calculated for any given temperature. The latter connects each index with the description of the corresponding energy level. Each energy level is described by the quantum numbers associated with the molecular group symmetry (Bunker & Jensen 1998), $C_{3v}(\text{M})$ for PH_3 and total angular momentum J . The quantum numbers for XY_3 molecules are quite complicated and have recently been discussed in detail for ammonia by Down et al. (2013). Our PH_3 quantum numbers follow the same general principles but are somewhat simpler since we neglect the possibility of a tunnelling mode.

Each energy level is described by the following quantum numbers :

$$n_1, n_2, n_3, n_4, L_3, L_4, L, \Gamma_{\text{vib}}, J, K, \Gamma_{\text{rot}}, \Gamma_{\text{tot}}, \quad (1)$$

where $L_3 = |l_3|$, $L_4 = |l_4|$, $L = |l|$, $K = |k|$. Here the vibrational quantum numbers n_1 (symmetric stretch), n_2 (symmetric bend), n_3 (asymmetric stretch) and n_4 (asymmetric bend) correspond to excitations of, respectively, the ν_1 , ν_2 , ν_3 and ν_4 modes. The doubly degenerate modes ν_3 and ν_4 require additional quantum numbers $L_3 = |l_3|$ and $L_4 = |l_4|$ describing the projections of the corresponding angular momenta (see Bunker & Jensen (1998)). The vibrational quantum number $L = |l|$, characterizes the coupling of l_3 and l_4 . The projection of the total vibrational angular momentum L is included to reduce ambiguity in the description of the energy levels, as it was in SYT (Sousa-Silva et al. 2013). Γ_{rot} , Γ_{vib} , and Γ_{tot} are, respectively, the symmetry species of the rotational, vibrational and total internal wave-functions in the molecular symmetry group $C_{3v}(\text{M})$, spanning A_1 , A_2 and E , where E is two-fold degenerate. J is the total angular momentum and $K = |k|$, $k = -J, \dots, J$ is the projection of the total angular momentum on the molecule fixed axis z . These twelve quantum numbers reduce ambiguity to the assignment of the energy levels. However, only J and Γ_{vib} are rigorous; at higher energies, energy states cannot necessarily be assigned unambiguous quantum labels. Apart from the quantum numbers we also provide the largest eigen-coefficient used to produce the theoretical assignment, see, for example, (Yurchenko & Tennyson 2014).

Since PH_3 transitions obey the strict selection rules $A_1 \leftrightarrow A_2$, $E \leftrightarrow E$, and $\Delta J = 0, \pm 1$, no higher J values were considered because $J = 45$ is the highest value of J for which there are eigenvalues exist below $8\,000\,\text{cm}^{-1}$, which is the highest lower energy threshold used in SAITY.

Excerpts from the energy and transition files are given in tables 1 and 2, respectively, with seven additional columns giving TROVE quantum numbers which are described in the supplementary data and by Sousa-Silva et al. (2013). As per the ExoMol convention, these are named SAITY.transitions and SAITY.states. The complete line list is freely available and can be downloaded from the Strasbourg data centre, CDS, via <ftp://cdsarc.u-strasbg.fr/pub/cats/J/MNRAS/> or from the ExoMol website, www.exomol.com. The website also offers the opportunity to download cross sections (Hill et al. 2013).

3 BACKGROUND TO THE CALCULATION

For this calculations we used a slightly refined version of the potential energy surface (PES) used for the SYT line list by (Sousa-Silva et al. 2013). This refinement was necessary because in our semi-empirical approach the refined PESs are ‘effective’ surfaces, inextricably connected to the size of the basis set. To achieve the accuracy and degree of completeness required of the SAITY line list, the present calculations used an increased basis set, so a refinement of the surface was

Table 1. Extract from the SALTY Energy file.

1	2	3	4	5	6	7	8	9	10	11	12	13	14	15	16	17	18	19	20	21	22
N	\tilde{E}	g_{tot}	J	Γ_{tot}	K	Γ_{rot}	L	n_1	n_2	n_3	n_4	L_3	L_4	Γ_{vib}	$ C_i ^2$	s_1	s_2	s_3	b_4	b_5	b_6
4770	18091.558811	8	0	2	0	1	3	0	3	6	1	2	1	2	1.00	1	3	2	3	0	1
4771	18108.514162	8	0	2	0	1	9	0	2	5	4	5	4	2	1.00	1	2	2	4	2	0
4772	18117.126945	8	0	2	0	1	3	0	3	6	1	2	1	2	1.00	1	3	2	3	0	1
4773	18141.236226	8	0	2	0	1	0	7	1	1	1	1	1	2	1.00	0	0	8	0	0	2
4774	18144.653263	8	0	2	0	1	3	0	4	5	2	5	2	2	1.00	1	2	2	2	4	0
4775	18180.965326	8	0	2	0	1	3	1	5	4	1	2	1	2	1.00	0	3	2	0	3	3
4776	18218.349734	8	0	2	0	1	0	0	4	4	4	4	4	2	1.00	1	2	1	0	5	3
4777	18287.993223	8	0	2	0	1	3	7	0	1	2	1	2	2	1.00	0	0	8	0	1	1
4778	18329.569862	8	0	2	0	1	6	0	6	1	9	1	5	2	1.00	0	0	1	0	15	0
4779	18393.321746	8	0	2	0	1	3	0	5	1	10	1	4	2	1.00	0	0	1	0	15	0
4780	18453.246434	8	0	2	0	1	3	0	5	1	10	1	4	2	1.00	0	0	1	0	15	0
4781	18506.447815	8	0	2	0	1	6	0	4	1	11	1	7	2	1.00	0	0	1	15	0	0
4782	18516.395845	8	0	2	0	1	3	6	0	3	0	3	0	2	1.00	8	0	1	0	0	0
4783	18548.610530	8	0	2	0	1	3	0	3	1	12	1	2	2	1.00	0	0	1	15	0	0
4784	18649.304702	8	0	2	0	1	6	0	4	1	11	1	7	2	1.00	0	0	1	15	0	0
4785	18725.969827	8	0	2	0	1	0	8	0	1	1	1	1	2	1.00	9	0	0	0	0	1
4786	19353.229098	8	0	2	0	1	6	0	7	1	9	1	7	2	1.00	0	0	1	16	0	0
4787	19493.996332	8	0	2	0	1	9	0	6	1	10	1	8	2	1.00	0	0	1	0	0	16
4788	19745.979241	8	0	2	0	1	0	8	1	1	1	1	1	2	1.00	9	0	0	0	0	2
4789	19894.271775	8	0	2	0	1	3	8	0	1	2	1	2	2	1.00	9	0	0	0	1	1
4790	20126.886789	8	0	2	0	1	3	7	0	3	0	3	0	2	1.00	9	0	1	0	0	0
4791	1118.304691	8	0	3	0	1	1	0	0	0	1	0	1	3	1.00	0	0	0	0	0	1
4792	2108.150565	8	0	3	0	1	1	0	1	0	1	0	1	3	1.00	0	0	0	0	0	2
4793	2234.920254	8	0	3	0	1	2	0	0	0	2	0	2	3	1.00	0	0	0	0	1	1
4794	2326.870042	8	0	3	0	1	1	0	0	1	0	1	0	3	1.00	0	0	1	0	0	0
4795	3085.609104	8	0	3	0	1	1	0	2	0	1	0	1	3	1.00	0	0	0	0	2	1
4796	3222.494320	8	0	3	0	1	2	0	1	0	2	0	2	3	1.00	0	0	0	3	0	0
4797	3311.958593	8	0	3	0	1	1	0	1	1	0	1	0	3	1.00	0	0	1	0	0	1
4798	3333.494686	8	0	3	0	1	1	0	0	0	3	0	1	3	1.00	0	0	0	2	1	0
4799	3424.626917	8	0	3	0	1	1	1	0	0	1	0	1	3	1.00	1	0	0	0	0	1
4800	3435.624836	8	0	3	0	1	2	0	0	1	1	1	1	3	1.00	0	0	1	0	0	1
4801	4050.520058	8	0	3	0	1	1	0	3	0	1	0	1	3	1.00	0	0	0	3	0	1
4802	4196.913916	8	0	3	0	1	2	0	2	0	2	0	2	3	1.00	0	0	0	0	2	2
4803	4283.755426	8	0	3	0	1	1	0	2	1	0	1	0	3	1.00	0	0	1	0	1	1
4804	4319.935065	8	0	3	0	1	1	0	1	0	3	0	1	3	1.00	0	0	0	4	0	0
4805	4408.422285	8	0	3	0	1	1	1	1	0	1	0	1	3	1.00	1	0	0	0	0	2
4806	4418.431045	8	0	3	0	1	2	0	1	1	1	1	1	3	1.00	0	0	1	0	0	2
4807	4438.012026	8	0	3	0	1	2	0	0	0	4	0	2	3	1.00	0	0	0	0	2	2
4808	4461.860840	8	0	3	0	1	4	0	0	0	4	0	4	3	1.00	0	0	0	2	1	1
4809	4517.161189	8	0	3	0	1	1	0	0	1	2	1	0	3	1.00	0	0	1	0	0	2
4810	4534.991076	8	0	3	0	1	2	1	0	0	2	0	2	3	1.00	1	0	0	0	1	1
4811	4545.384096	8	0	3	0	1	1	0	0	1	2	1	2	3	1.00	0	0	1	0	1	1

Column	Notation	
1	N	Energy level reference number (row)
2	\tilde{E}	Term value (in cm^{-1})
3	g_{tot}	Total degeneracy
4	J	Rotational quantum number
5	Γ_{tot}	Total symmetry in $C_{3v}(\text{M})$
6	K	Rotational quantum number, projection of J onto the z -axis
7	Γ_{rot}	Symmetry of the rotational contribution in $C_{3v}(\text{M})$
8	L	The projection of the total vibrational angular momentum
9,10,11,12	$n_1 - n_4$	Normal mode vibrational quantum numbers
13,14	L_3, L_4	projections of the angular momenta corresponding to n_3 and n_4
15	Γ_{vib}	Symmetry of the vibrational contribution in $C_{3v}(\text{M})$
16	$ C_i ^2$	Largest contribution used in the assignment
17,18,19,20,21,22	$s_1, s_2, s_3, b_1, b_2, b_3$	Local mode vibrational quantum numbers

Table 2. Extract from the SALT Transition file.

F	I	A_{IF} / s^{-1}
4220641	4736989	9.0696e-04
8442759	8640461	5.3636e-05
1269889	1056999	5.5676e-04
4631869	4737012	2.3014e-04
4632512	4737066	9.6883e-04
614599	820125	1.0712e-03
3549641	3825894	9.3653e-04
8085571	7937418	5.3630e-07
2304706	2606502	2.4236e-03
3829402	3545923	1.0250e-04
1750096	1497115	2.3840e-04
823228	612463	4.8085e-07
7589341	7582878	8.6990e-04
507260	612492	5.5009e-04
6611560	6605474	2.2927e-04
2306005	2300595	1.8031e-04
5869339	5986016	1.5085e-04
870236	1057299	4.1518e-04

F : Upper state counting number; I : Lower state counting number; A_{IF} : Einstein A coefficient in s^{-1} .

necessary. It was done by performing a least square fit to available experimental ro-vibrational energies of PH_3 with the rotational quantum numbers $J = 0, 1, 2, 3, 4$, mostly taken from the HITRAN database.

The PES parameters used here are given as Supplementary Material to this paper in the form of a Fortran 95 program. It should be noted that this is also an ‘effective’ PES and guarantees to give accurate results only in conjunction with the same method and basis set used to produce it with.

As with the SYT PH_3 line list, the variational rotation-vibration program suite TROVE (Yurchenko et al. 2007) was employed for all nuclear motion calculations for SALT. The application of variational methods to polyatomic molecules requires increasingly large Hamiltonian matrices to be diagonalised, which is very computationally demanding and until recently prohibitively so. With the power and parallelism of modern computers, it is now possible to use this method for the production of accurate spectra.

To accommodate the higher demands of the present line list, a larger basis set was used, with a corresponding higher polyad number. The polyad number controls the size of the basis sets at all contraction steps using the polyad-truncation scheme (Ovsyannikov et al. 2008b), defined by

$$P = 2(s_1 + s_2 + s_3) + b_1 + b_2 + b_3 \leq P_{\max}, \quad (2)$$

where s_i and b_i are the primitive quantum numbers associated with the basis functions, ϕ_{s_i} and ϕ_{b_i} , for the stretching modes and the bending modes, respectively. Here TROVE (Yurchenko et al. 2007) constructs a synthetic line list for $^{31}\text{PH}_3$ in its ground electronic state. To this end the Schrödinger equation for the rotation-vibration motion of nuclei is solved to obtain eigenvalues (ro-vibrational energies) and eigenfunctions (nuclear motion wavefunctions). The latter are necessary for ro-vibrational averaging of the dipole moment of the rotating molecule and thus to compute the transitional probabilities, usually expressed in terms of the Einstein coefficients or line strengths following the description by Yurchenko et al. (2005a). Our basis set contains two contributions, (i) all basis functions with the primitive quantum numbers satisfying $P \leq 16$ and (ii) stretching functions ranging up to $P = 20$ but with some high P -polyad ($P \geq 17$) stretching contributions that couple all three stretching modes removed. Increasing the polyad number is computationally costly, and as such the increased coverage of the stretching excitations only was motivated by assumption that the stretching excitations produce the strongest transitions. The larger basis set guarantees a better convergence for the present calculations, but requires the PES to be refined to the new basis set, as discussed above. The $J = 0$ Hamiltonian matrices were then constructed, and the empirical basis set correction scheme (EBSC) of Yurchenko et al. (2009) was

Table 3. Observed bands centres, from HITRAN (Rothman et al. 2013), and standard deviation, σ , with which the TROVE calculations reproduce the terms within each band. The first three columns give integrated band intensity for each band calculated for SYT, SAITY and HITRAN.

Band	Band Centre (cm ⁻¹)	σ (cm ⁻¹)		Band Intensity (cm / molecule)		
		SYT	SAITY	HITRAN	SYT	SAITY
ν_2	992.135	0.020	0.015	3.087×10^{-18}	3.264×10^{-18}	3.261×10^{-18}
ν_4^1	1118.307	0.005	0.003	3.149×10^{-18}	3.436×10^{-18}	3.436×10^{-18}
$2\nu_2$	1972.571	0.007	0.004	9.390×10^{-21}	1.414×10^{-20}	1.468×10^{-20}
$\nu_2 + \nu_4^1$	2108.152	0.034	0.013	9.504×10^{-20}	1.484×10^{-19}	1.487×10^{-19}
$2\nu_4^0$	2226.835	0.010	0.008	4.689×10^{-19}	7.684×10^{-19}	7.590×10^{-19}
$2\nu_4^2$	2234.915	0.014	0.005	combined above	combined above	combined above
ν_1	2321.121	0.012	0.008	4.926×10^{-18}	6.091×10^{-18}	6.127×10^{-18}
ν_3^1	2326.867	0.013	0.008	1.454×10^{-17}	1.650×10^{-17}	1.648×10^{-17}
$3\nu_2$	2940.767	0.046	0.032	6.725×10^{-21}	2.127×10^{-20}	2.129×10^{-20}
$\nu_2 + 2\nu_4^0$	3214.936	0.024	0.017	3.612×10^{-21}	7.478×10^{-21}	6.996×10^{-21}
Overall		0.020	0.012			

applied. Here, band centre values from the ro-vibrational calculations are replaced with extremely accurate corresponding experimental values, or deviated towards these values. This is performed iteratively, until the entire band is considered to be optimal. At the end of this correction, the rms deviation for the bands whose centre had been replaced went from an rms deviation of 0.02 cm^{-1} in SYT to 0.012 cm^{-1} in SAITY. This improvement may reflect the better use of EBSC, but overwhelmingly is due to the use of the enhanced PES. Table 3 gives a band-by-band summary of this improvement. The $2\nu_4$ and $\nu_2 + \nu_4$ bands were particularly responsive to this process. Further details of the TROVE computational procedure are given by Sousa-Silva et al. (2013).

Table 3 also compares the integrated band intensity computed for the SYT and SAITY line lists with those obtained from HITRAN 2012. In each case, the band intensity was computed by explicit summation of the intensities at 296 K of all lines within a band. The two $2\nu_4$ bands were considered together since it is difficult to disentangle their transitions. The band intensities for the two computed lists are very similar. They are both in reasonable agreement with, but somewhat larger than, HITRAN; given the greater completeness of the computed linelists, it is to be expected that this method would yield somewhat larger band intensities.

For the rotational spectra from CDMS the integrated intensity is $1.214 \times 10^{-18} \text{ cm/molecule}$ which is very similar to SAITY's 1.218×10^{-18} . One further test on the intensities was performed. Given that the intensity of weak lines can be highly sensitive to the choice of wavefunction (Tennyson 2014), and hence the underlying PES, an explicit comparison was made between SYT and SAITY of the intensities of the weak, forbidden lines with $\Delta K = 3$. These were found to be very little changed for the individual transitions inspected, with the integrated intensity for all these transitions going from $5.53 \times 10^{-19} \text{ cm / molecule}$ in SYT to $5.60 \times 10^{-19} \text{ cm / molecule}$ in SAITY. In practice variational procedures, such as those use here, have long been used to get reliable predicted intensities for such transitions (Miller et al. 1990; Lodi & Tennyson 2008).

As well as employing a larger basis set than before, this line list extends SYT by using (i) a larger energy level range of $E_{\text{max}} \leq 18\,000 \text{ cm}^{-1}$ (instead of $\leq 12\,000 \text{ cm}^{-1}$), (ii) wider frequency range of $0 - 10\,000 \text{ cm}^{-1}$ (instead of $0 - 8\,000 \text{ cm}^{-1}$) and (iii) rotational excitations considered up to $J_{\text{max}} = 46$ (instead of 34). This expansion is necessary to guarantee accuracy and completeness at high temperatures, but it makes the calculation of the line list much more computationally demanding.

The diagonalisation of the matrices involved in the variational procedure corresponding to high values of J is the most computationally demanding part of a line list calculation, as it requires substantial memory, long runs and requires

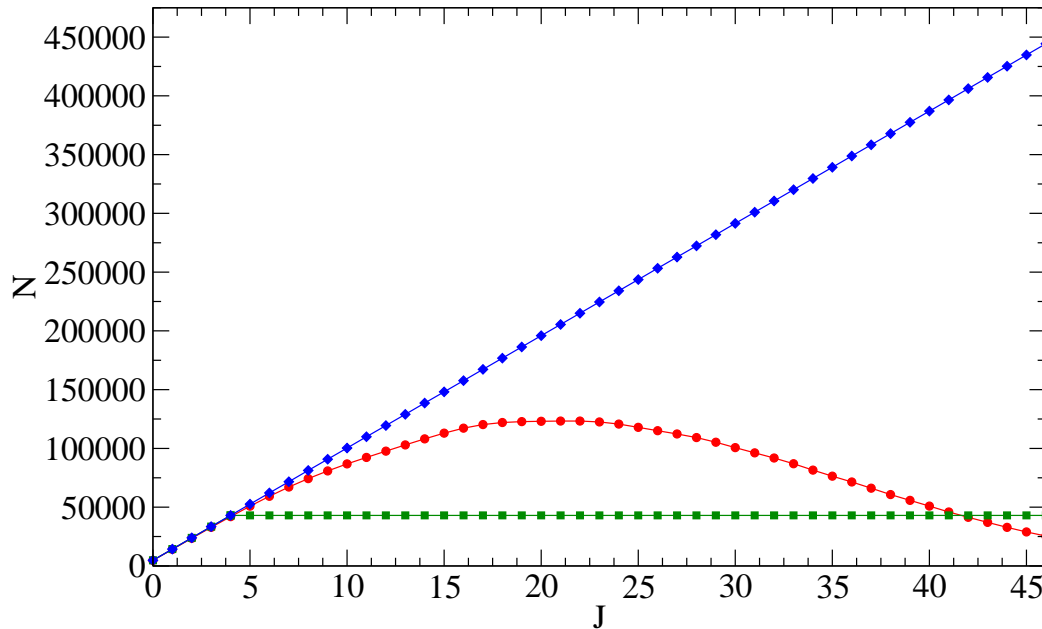


Figure 1. Dimensions of the E -symmetry matrices with J (blue diamonds), the corresponding number of eigenvalues below $18\,000\text{ cm}^{-1}$ (red circles) and number of non-zero elements on each row (green squares).

MPI to diagonalise efficiently. A variety of strategies were used to deal with this. The dimension of the matrices of the symmetries scales approximately as 1:1:2, for A_1 , A_2 and E , respectively.

The largest matrix to be diagonalised for SAITY ($J = 46$, E symmetry) has dimensions of 444 726. As can be seen from Fig. 3, the size of the ro-vibrational matrices scales linearly with J , but the number of non-zero elements and the number of eigenvalues under the energy threshold for the line list ($8\,000\text{ cm}^{-1}$) do not. The size of the matrices grows roughly with $N_{J=0}^\Gamma \times (2J + 1)$, where $N_{J=0}^\Gamma$ is the dimension of the matrix block for $J = 0$. For the symmetry with the biggest matrices, $\Gamma = E$, $N_{J=0}^E = 4778$.

The initial (low J) matrices were sufficiently small to employ the standard LAPACK eigensolver DSYEV (Anderson et al. 1999) to solve the full eigenvalue problem, and this was used for all $J \leq 16$ and 9 (A and E symmetries, respectively). As the matrices increased in size, memory constraints required the MPI version PDSYEV of this eigensolver to be used on large shared memory systems (COSMOS) in order to cope with the size of these matrices. We also successfully explored the openmp PLASMA library Kurzak et al. (2013) for the matrices with dimensions between 100 000 and 200 000.

Using these three eigensolvers, all eigenvalues and eigenvectors were computed for $J \leq 46$, using the energy threshold of $18\,000\text{ cm}^{-1}$, totalling 7 480 690 energy levels.

A high quality dipole moment surface (DMS) is a prerequisite for correctly computing the transition moments used to generate the Einstein A coefficients and in turn accurate line intensities; Tennyson (2014) gives a discussion of the issues involved in this. The DMS used here is completely theoretical, an approach that has been shown to yield results competitive with experiment (Lynas-Gray et al. 1995), and has already been used in the SYT line list where it provided intensities in good agreement with experiment. It is a six-dimensional *ab initio* (CCSD(T)/aug-cc-pVTZ) electric dipole moment surface, calculated on a grid of 10 080 molecular geometries, and it is described in further detail

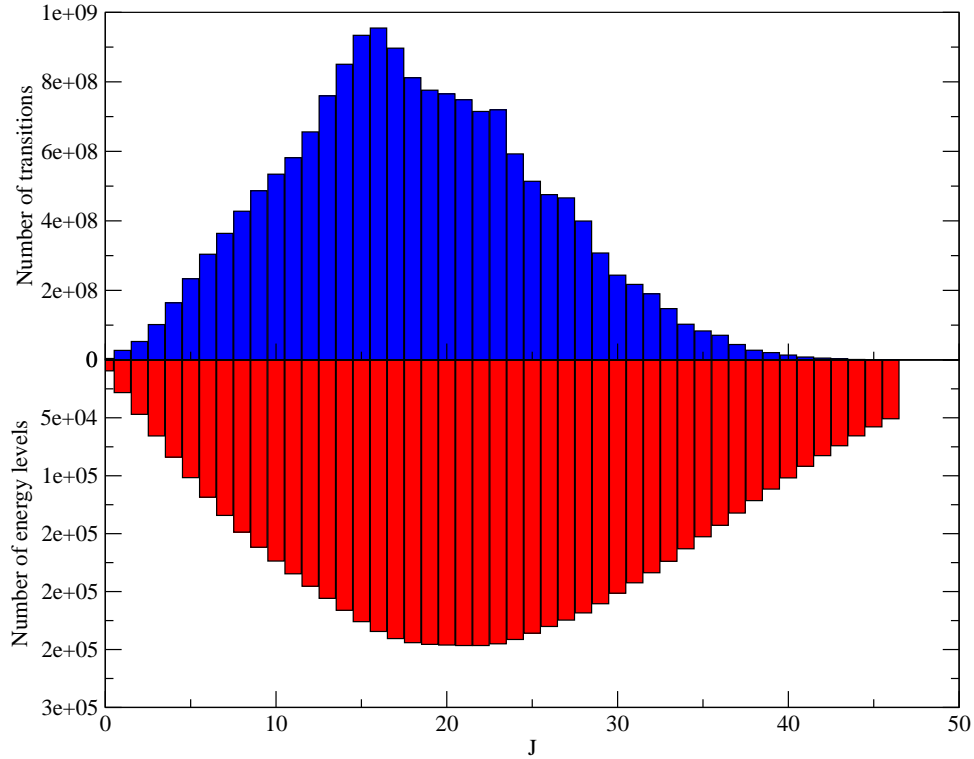


Figure 2. Number of energy levels in each rotational quantum number, J , and transitions between J and $J, J + 1$ in the SAITY line list, summed over all symmetries.

elsewhere (Yurchenko et al. 2006). To reduce the size of the computation, only eigen-coefficients of the upper states with a magnitude larger than 10^{-14} were selected.

Despite matrix diagonalization utilising the most computational resources, it is the computation of transition intensities that actually dominates the total computer time. However this step has the advantage that it is easily parallellised and spread over many processors, and indeed computer systems. As shown in Fig. 3, the number of transitions between energy levels peaks between $J = 15$ and 18 , so this was the region that corresponded to the most expensive part of the intensity calculations, accounting for about 17% of the total transitions. The number of transitions does not correlate smoothly with J pairs due to the different way A and E symmetries are affected by J , particularly for values of K that are multiples of 3.

Employing CPUs available to us at the HPC centres DiRAC@Darwin and DiRAC@COSMOS, TROVE was used to calculate the intensities across almost all symmetries and J values. However this proved slow and computationally expensive, so for some of the particularly computationally demanding sections, a newly-developed graphical processor unit (GPU) implementation of the TROVE program was employed. This allowed us to use multiple GPUs to compute multiple initial states simultaneously, effectively reducing computing time by over an order of magnitude. This was used to compute the absolute intensities for most A symmetry transitions with $J \geq 20$, on the Emerald cluster. The algorithm employed will be described elsewhere (Al-Refaie et al. 2015).

After this work was completed, Nikitin et al. (2014) published a detailed analysis of *ab initio* methods for calculating the phosphine DMS. In general the agreement between their predictions and ours is very good.

Table 4. Maximum temperatures for which the SALT line list is percentually complete.

T_{\max} (K)	Completeness %
1014	100
1146	99
1797	80
1500	91
2000	70
2500	50

4 LINE LIST VALIDATION AND TEMPERATURE DEPENDENCE

Line lists do not specify a temperature, since the Einstein coefficients for the transitions are independent of temperature. SALT can only be considered a ‘hot’ line list because its energy and rotational excitation thresholds ensure that all those states that are significantly populated up to $T = T_{\max}$ are used to produce the catalogue of transitions.

To model the spectrum of phosphine at different temperatures, the line intensities are calculated using:

$$I(f \leftarrow i) = \frac{A_{if}}{8\pi c} g_{\text{ns}}(2J_f + 1) \frac{\exp\left(-\frac{E_i}{kT}\right)}{Q \tilde{\nu}_{if}^2} \left[1 - \exp\left(-\frac{hc\tilde{\nu}_{if}}{kT}\right) \right], \quad (3)$$

where k is the Boltzmann constant, T the absolute temperature and g_{ns} is the nuclear spin statistical weight factor. Q , the partition function, is given by:

$$Q = \sum_i g_i \exp\left(-\frac{E_i}{kT}\right), \quad (4)$$

where g_i is the degeneracy of a particular state i with energy E_i . For PH_3 , g_i is $g_{\text{ns}}(2J_i + 1)$ with $g_{\text{ns}} = 8$ for all A_1 , A_2 and E symmetries.

Previous work has looked in depth at the temperature dependent partition function of phosphine (Sousa-Silva et al. 2014). This work produced accurate and fully converged values for the partition function for temperatures below 3000 K by the explicit summation of theoretical rotation-vibration energy levels of the molecule. The convergence dependence on temperature arises due to the growing contribution higher states make towards the value of the partition function as temperature increases. To achieve this convergence, 5.6 million energy levels with high accuracy were used, combined with an additional 145 million calculated with an accurate vibrational component but with the rotational contribution estimated by a rigid rotor approximation, and consequently with a much decreased level of accuracy. However, the rotational states are anchored to the vibrational states, so an accurate vibrational description means that the energy level clusters remain valid (Yurchenko et al. 2005b), even if the degradation of accuracy from the rotational component makes the energies within the cluster only approximate. Consequently, their collective contribution to the partition function and related properties remains correct.

The T_{\max} for which molecular data is complete to a satisfactory degree can be found by computing the temperature-dependent partition function using only the energy levels under the lower energy threshold considered in the line list (here 8 000 cm^{-1}), and then comparing its value to that of the complete partition function. By considering the ratio $Q_{\text{limit}}/Q_{\text{total}}$, where Q_{total} is the converged partition function value calculated by explicitly summing over all energy levels and Q_{limit} is the partition function calculated using only those levels with energies up to SALT’s threshold of 8 000 cm^{-1} . Fig. 4 shows SALT’s completeness with increasing temperature. As can be seen from the Table 4, SALT is over 90% complete for temperatures below 1500 K, but quickly becomes depleted at higher temperatures. It is possible to use SALT to model temperatures over 1500 K by using the percentual loss of completeness to estimate the proportion of opacity missing from a spectrum (Neale et al. 1996), but it is recommended that 1500 K is taken as a soft limit to the applicability of the SALT line list.

Using the equations above and the present line list, multiple cross-sections were simulated for PH_3 . Figures 4 and

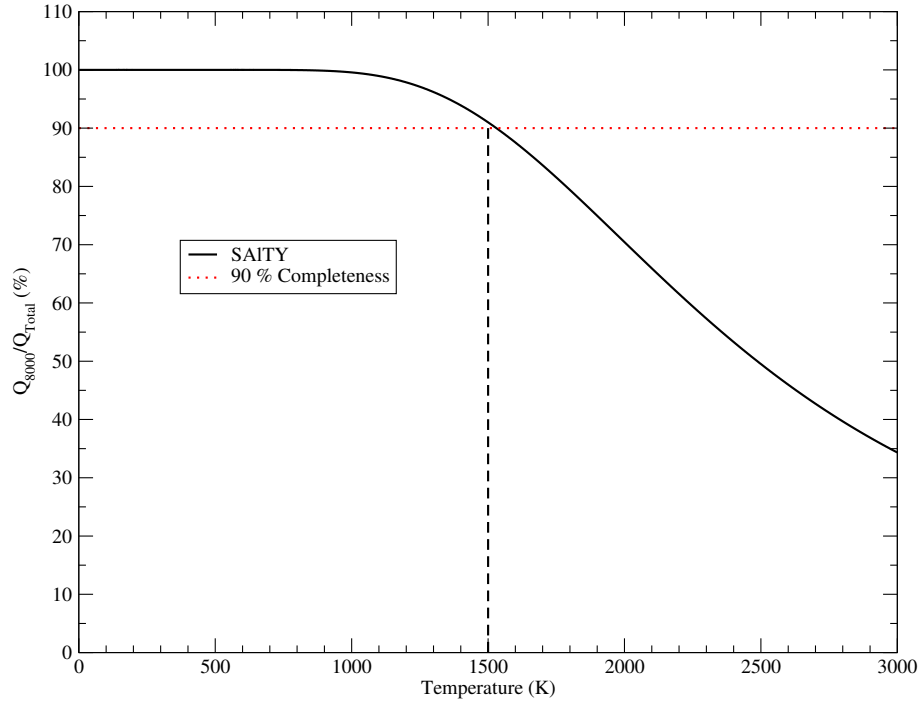


Figure 3. Ratio of effective partition function used in SAITY, Q_{8000} , to the converged value, Q_{total} , calculated in Sousa-Silva et al. (2014). This ratio gives a measure of completeness of SAITY as a function of temperature.

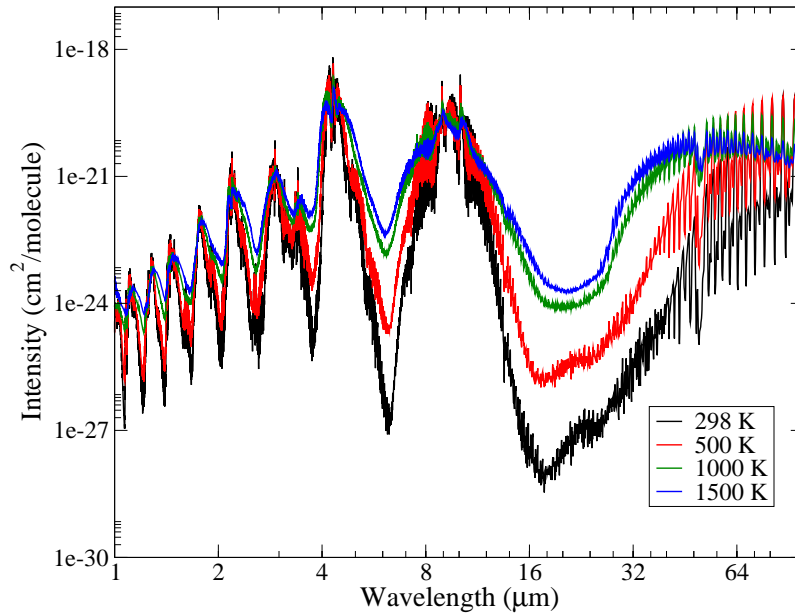


Figure 4. Overview of the full SAITY spectrum of PH_3 for $T = 300, 500, 1000$ and 1500 K, absorption cross-sections ($\text{cm}^2/\text{molecule}$) with $\text{HWHM} = 0.5 \text{ cm}^{-1}$. Looking at the minimum of the spectra, the cross-sections are ordered in increasing temperature.

5 illustrate the temperature dependence of phosphine for $T = 300, 500, 1000, 1500$ and 2000 K. It can be seen that the spectra at higher temperatures have less features and a loss of sharp Q -branches. Figure 5, part **c**, covers the wavelength region $3.8 - 5.1 \text{ } \mu\text{m}$ which, as mention above, is of particular importance for the spectral characterisation of brown dwarfs and gas giants.

Fig. 6 demonstrates how the density of lines per an absorption intensity $I_{if} = A \times 10^x$ unit changes with temperature, covering the whole wavenumber range $0 - 10\,000 \text{ cm}^{-1}$. As the temperature rises, the number of intense lines increases but

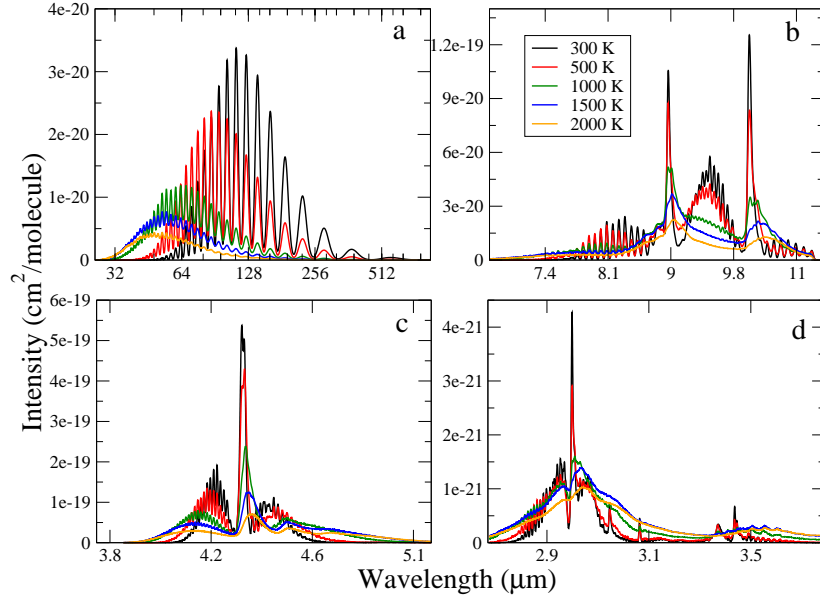


Figure 5. SALTY absorption spectra of PH_3 for $T = 300, 500, 1000, 1500$ and 2000 K, convoluted with a Gaussian profile, $\text{HWHM} = 2 \text{ cm}^{-1}$, for the 30(a), 10(b), 5(c) and 3(d) μm regions

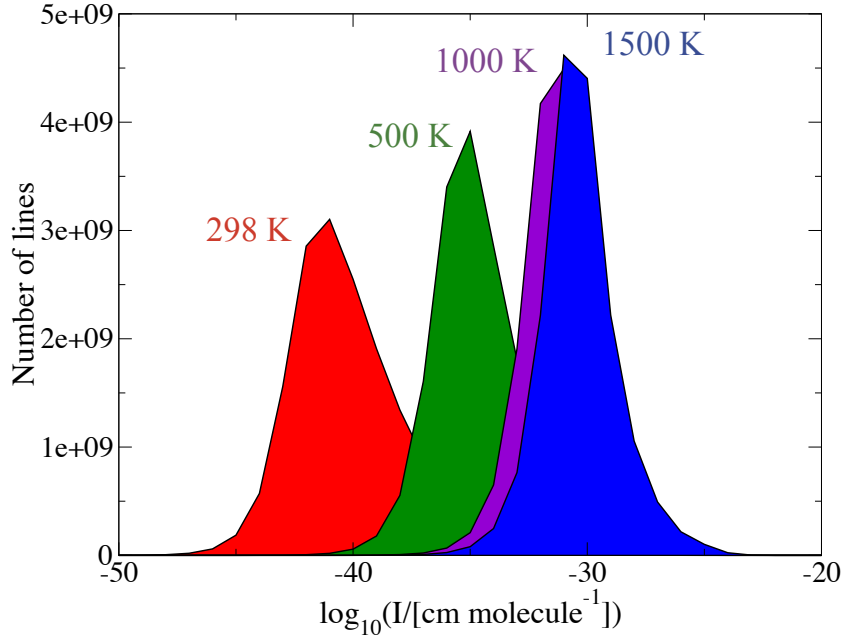


Figure 6. Number of intense lines as a function of intensity for different temperatures. The x -axis gives the log of the intensity in $\text{cm}^2/\text{molecule}$, while the y -axis represents the number of transitions per each $10^x \text{ cm}^2/\text{molecule}$ bin.

the range of intensities in the spectrum becomes narrower. The Gaussian-like intensity distributions peak at $I = 10^{-41}$, $= 10^{-35}$, $= 10^{-31}$, and $= 10^{-31}$ for $T = 298, 500, 1000$, and 1500 K, respectively. This is different from the intensity distribution found for CH_4 by Yurchenko & Tennyson (2014), where the proportion of strong lines was found to be much larger.

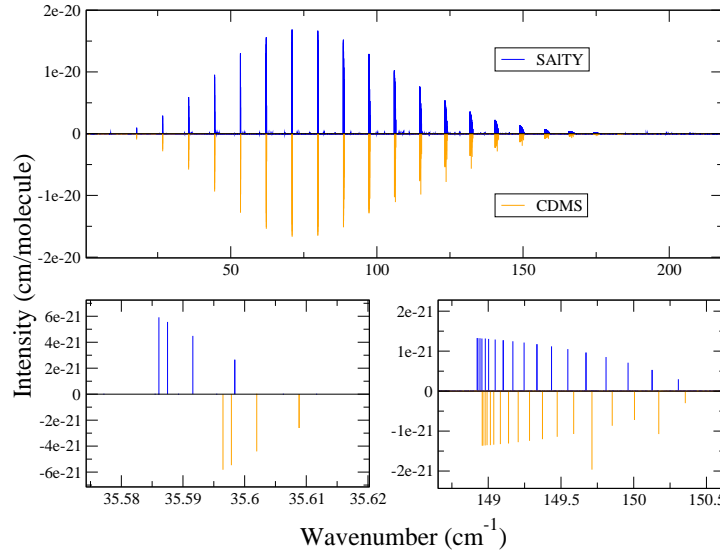


Figure 7. Comparison of the SAITY line list with the most recent phosphine data from CDMS at room temperature (Müller 2013).

4.1 Comparison with experiment

Sousa-Silva et al. (2013) offers a detailed comparison of SYT to the existing experimental data, where it was found that it replicates very well the observed phosphine spectra at room temperature, with a maximum rms deviation from CDMS (Müller et al. 2005; Müller 2013) of 0.076 cm^{-1} for the rotational spectrum and of 0.23 cm^{-1} from HITRAN (Rothman et al. 2013). As can be seen from Fig. 8, the SAITY line list is also in excellent agreement with HITRAN (and incorporated CDMS data), and it is expected that SAITY will have slightly lower rms deviations from experiment at this temperature.

The most recent CDMS update (Müller 2013) contains a very comprehensive description of the pure rotational band of phosphine. Figure 7 demonstrates that SAITY is in excellent agreement with the CDMS data. The transitions in the bottom left box shows a deviation of approximately 0.01 cm^{-1} , while the right most box, at higher wavenumbers, shows a deviation of approximately 0.04 cm^{-1} .

The apparent intensity disagreements with HITRAN occur because of an overestimation of the intensity of some of the degenerate $A_1 \leftrightarrow A_2$ transitions which are in such close proximity that they have been perceived as one doubly strong transition in the experimental data. This has been partially resolved by Malathy Devi et al. (2014), who corrected these intensities for the region 1950 to 2450 cm^{-1} . The bottom left box in figure 8 includes this data, and it can be seen SAITY is in much better agreement with it than with the HITRAN data. We recommend that the Malathy Devi et al. (2014) data should be included in the next release of HITRAN.

The data in HITRAN are generally very accurate for room temperature simulations. However, if the current HITRAN database is used to simulate high temperature spectra, the differences become much more striking, as can be seen in Fig. 9.

The only available data above 300 K comes from the Pacific Northwest National Laboratory (PNNL) who provide cross-sections for PH_3 up to temperatures of 323 K (Sharpe et al. 2004). Comparisons with SAITY for $T = 50 \text{ C}$, or 323 K , can be seen in Fig. 10. The PNNL data is approximately 8% weaker than SAITY's, but both are otherwise in good agreement. Given its larger density and coverage, it is recommended that SAITY is used to simulate cross-sections, even at low temperatures.

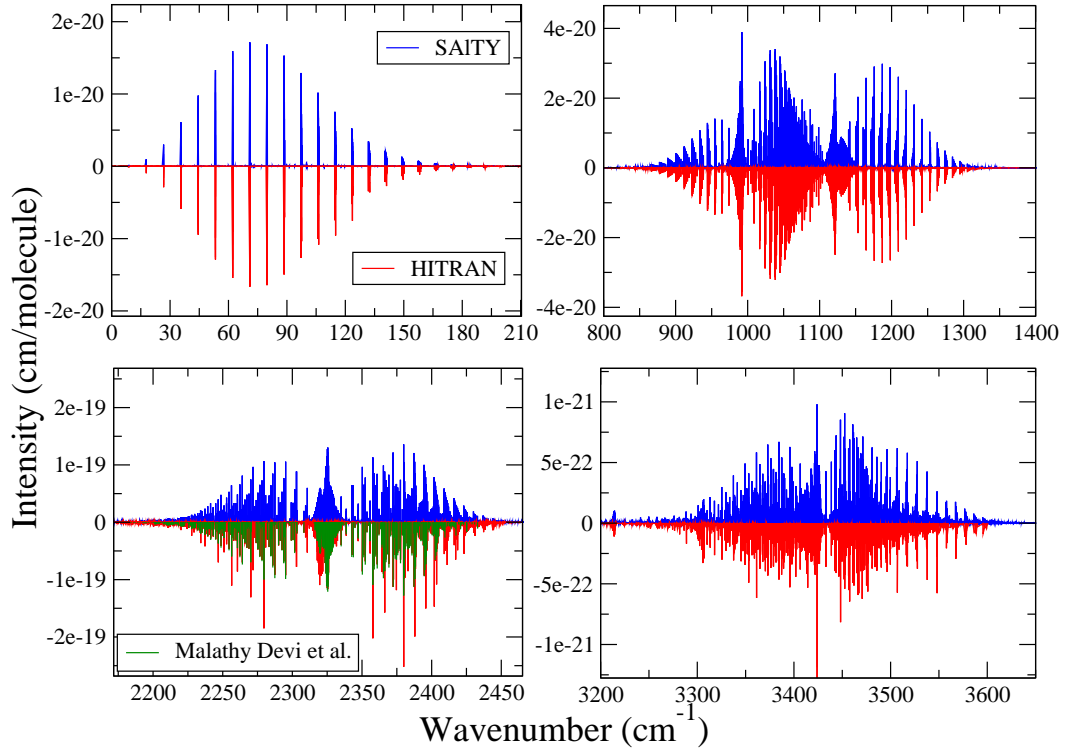


Figure 8. Comparison of the SAITY line list with the phosphine data from HITRAN (Rothman et al. 2013) at room temperature; also shown are the recent results of Malathy Devi et al. (2014).

5 CONCLUSION

An accurate and comprehensive line list for phosphine is presented, which has been called SAITY. It contains 16.8 billion transitions between 7.5 million energy levels and it is suitable for simulating spectra up to temperatures of 1500 K.

Its only limitations are: upper states with energies above $18\,000\text{ cm}^{-1}$ are excluded, and there is an effective short-end wavelength cut-off of $1\text{ }\mu\text{m}$, which is an unimportant region for PH_3 . SAITY improves on the previous room temperature phosphine line list SYT in terms of the size of the basis set, corresponding refined potential energy surface and increased spectral range. It is therefore recommended that SAITY is used for all applications, even at low temperatures where SYT would provide reasonable results.

The tunnelling effect present in ammonia is predicted in phosphine but has yet to be observed in phosphine (Belov et al. 1981), due to its much higher inversion barrier ($12\,300\text{ cm}^{-1}$). This tunnelling effect is not considered here, but rough preliminary calculations have predicted the position, size and intensity of transitions from split energy levels. Further work on this effect will be published elsewhere.

The SAITY line list is presented as the latest in a series of molecules as part of the ExoMol project, which aims to provide comprehensive line lists for every molecule relevant to the characterisation of the atmospheres of cool stars and exoplanets. SAITY is freely available online in full or filtered by wavelength and intensity, from the ExoMol website. The line list in its entirety is very large but can be made more manageable by using cross sections (Hill et al. 2013) (available at ExoMol) or k -coefficients (Irwin et al. 1996).

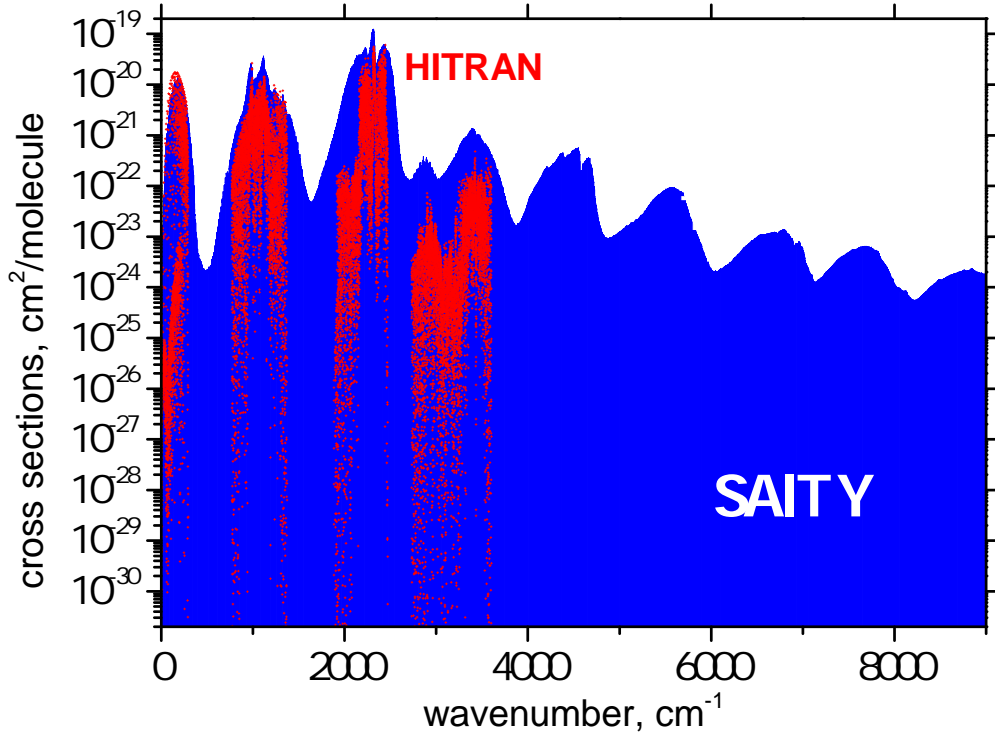


Figure 9. Comparison of the SAITY line list with the phosphine data from HITRAN (Rothman et al. 2013) at 1500 K.

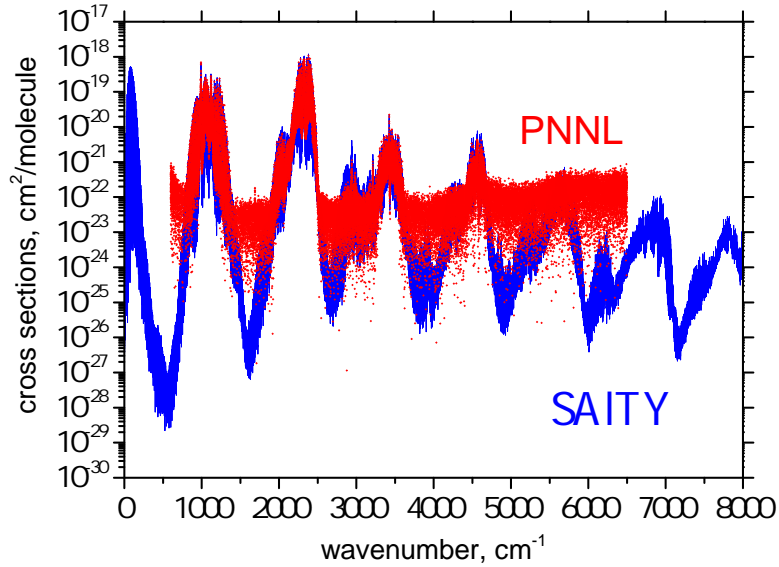


Figure 10. Comparison of the SAITY absorption cross-sections for PH_3 with PNNL and HITRAN at $T = 50$ C, $\text{HWHM} = 0.076$ cm^{-1} .

ACKNOWLEDGEMENTS

This work was supported by the ERC Advanced Investigator Project 267219. The research made use of the DiRAC@Darwin, DiRAC@COSMOS and the EMERALD HPC clusters. DiRAC is the UK HPC facility for particle physics, astrophysics and cosmology and is supported by STFC and BIS. The COSMOS Shared Memory system at DAMTP, University of Cambridge operated on behalf of the STFC DiRAC HPC Facility. This equipment is funded by BIS National E-infrastructure capital grant ST/J005673/1 and STFC grants ST/H008586/1, ST/K00333X/1. The EMERALD High Performance Computing facility is provided via the Centre for Innovation (Cfi). The Cfi is formed from the Universities of Bristol, Oxford, Southampton and UCL in partnership with STFC Rutherford Appleton Laboratory. We thank James Briggs (COSMOS) and Cheng Liao (SGI) for their help with the PLASMA eigensolver.

The authors would also like to thank Duncan A. Little, Hannah Lees, Sally Hewett, Helen Parks, Antonio Silva, Antonio S. Silva and Peter J. Day for their support and contribution.

REFERENCES

- Agundez M., Cernicharo J., Decin L., Encrenaz P., Teyssier D., 2014, *ApJ*, 790, L27
- Ainetschian A., Haring U., Spiegl G., Kreiner W. A., 1997, *J. Mol. Spectrosc.*, 181, 99
- Al-Rafaie A. F., Yurchenko S. N., Yachmenev A., Tennyson J., 2014, *MNRAS*
- Al-Rafaie A. F., Yurchenko S. N., Tennyson J., 2015, *Comput. Phys. Commun.*, (to be submitted)
- Anderson E. et al., 1999, *LAPACK Users' Guide*, 3rd edn. Society for Industrial and Applied Mathematics, Philadelphia, PA
- Baldacci A., Malathy Devi V., Narahari Rao K., Tarrago G., 1980, *J. Mol. Spectrosc.*, 81, 179
- Barber R. J., Tennyson J., Harris G. J., Tolchenov R. N., 2006, *MNRAS*, 368, 1087
- Belov S. P., Burenin A. V., Polyansky O. L., Shapin S. M., 1981, *J. Mol. Spectrosc.*, 90, 579
- Brown L. R., Sams R. L., Kleiner I., Cottaz C., Sagui L., 2002, *J. Mol. Spectrosc.*, 215, 178
- Bunker P. R., Jensen P., 1998, *Molecular Symmetry and Spectroscopy*, 2nd edn. NRC Research Press, Ottawa
- Butler R. A. H., Sagui L., Kleiner I., Brown L. R., 2006, *J. Mol. Spectrosc.*, 238, 178
- Cazzoli G., Puzzarini C., 2006, *J. Mol. Spectrosc.*, 239, 64
- Chu F. Y., Oka T., 1974, *J. Chem. Phys.*, 60, 4612
- Davies P. B., Neumann R. M., Wofsy S. C., Klemperer W., 1971, *J. Chem. Phys.*, 55, 3564
- Down M. J., Hill C., Yurchenko S. N., Tennyson J., Brown L. R., Kleiner I., 2013, *J. Quant. Spectrosc. Radiat. Transf.*, 130, 260
- Edgington S. G., Atreya S. K., Trafton L. M., Caldwell J. J., Beebe R. F., Simon A. A., West R. A., Barnet C., 1998, *Icarus*, 133, 192
- Encrenaz T. et al., 2014, *EPSC*, 9
- Fegley Jr B., Lodders K., 1996, *ApJ*, 472, L37
- Fletcher L. N., Orton G. S., Teanby N. A., Irwin P. G. J., 2009, *Icarus*, 202, 543
- Fusina L., Di Lonardo G., 2000, *J. Mol. Spectrosc.*, 517, 67
- He S. G., Zheng J. J., Hu S. M., Lin H., Ding Y., Wang X. H., Zhu Q. S., 2001, *J. Chem. Phys.*, 114, 7018
- Helminger P., Gordy W., 1969, *Phys. Rev.*, 188, 100
- Helms D. A., Gordy W., 1977, *J. Mol. Spectrosc.*, 66, 206
- Hill C., Yurchenko S. N., Tennyson J., 2013, *Icarus*, 226, 1673
- Hinshelwood, Topley, 1924, *Journal of the Chemical Society, Transactions*, 125, 393
- Irwin P. G. J., Calcutt S. B., Taylor F. W., Weir A. L., 1996, *J. Geophys. Res.-Planets*, E101, 26137

- Kshirsagar R. J., 2007, *J. Mol. Spectrosc.*, 241, 116
- Kurzak J. et al., 2013, *Multicore Computing: Algorithms, Architectures, and Applications*, 119
- Lodi L., Tennyson J., 2008, *J. Quant. Spectrosc. Radiat. Transf.*, 109, 1219
- Loomis C., Strandberg M. W. P., 1951, *Phys. Rev.*, 81, 798
- Lynas-Gray A. E., Miller S., Tennyson J., 1995, *J. Mol. Spectrosc.*, 169, 458
- Maciá E., 2005, *Chemical Society Reviews*, 34, 691
- Malathy Devi V., Kleiner I., Sams R. L., Brown L. R., Benner D. C., Fletcher L. N., 2014, *J. Mol. Spectrosc.*, 298, 11
- Miller S., Tennyson J., Sutcliffe B. T., 1990, *J. Mol. Spectrosc.*, 141, 104
- Moreno R., Marten A., Lellouch E., 2009, in *AAS/Division for Planetary Sciences Meeting Abstracts# 41*, Vol. 41
- Morley C. V., Marley M. S., Fortney J. J., Lupu R., Saumon D., Greene T., Lodders K., 2014, *ApJ*, 787, 78
- Moses J. I., 2014, *Phil. Trans. Royal Soc. London A*, 372, 20130073
- Müller H. S., 2013, *J. Quant. Spectrosc. Radiat. Transf.*, 130, 335
- Müller H. S. P., Schlöder F., Stutzki J., Winnewisser G., 2005, *J. Molec. Struct. (THEOCHEM)*, 742, 215
- Neale L., Miller S., Tennyson J., 1996, *ApJ*, 464, 516
- Nikitin A. V., Holka F., Tyuterev V. G., Fremont J., 2009, *J. Chem. Phys.*, 130, 244312
- Nikitin A. V., Rey M., Tyuterev V. G., 2014, *J. Mol. Spectrosc.*, , (in press)
- Nixon C. A., Teanby N. A., Irwin P. G., Hörst S. M., 2013, *Icarus*, 224, 253
- Noll K. S., Marley M. S., 1997a, in *Planets Beyond the Solar System and the Next Generation of Space Missions*, Vol. 119, p. 115
- Noll K. S., Marley M. S., 1997b, in *Planets Beyond the Solar System and the Next Generation of Space Missions*, Vol. 119, p. 115
- Ovsyannikov R. I., Thiel W., Yurchenko S. N., Carvajal M., Jensen P., 2008a, *J. Mol. Spectrosc.*, 252, 121
- Ovsyannikov R. I., Thiel W., Yurchenko S. N., Carvajal M., Jensen P., 2008b, *J. Chem. Phys.*, 129, 044309
- Owen T., Encrenaz T., 2003, in *Solar System History from Isotopic Signatures of Volatile Elements*, Springer, pp. 121–138
- Pickett H. M., Poynter R. L., Cohen E. A., 1981, *J. Quant. Spectrosc. Radiat. Transf.*, 26, 197
- Prinn R. G., Lewis J. S., 1975, *Science*, 190, 274
- Rothman L. S. et al., 2013, *J. Quant. Spectrosc. Radiat. Transf.*, 130, 4
- Rothman L. S. et al., 2010, *J. Quant. Spectrosc. Radiat. Transf.*, 111, 2139
- Salem J., Aroui H., Bouanich J. P., Walrand J., Blanquet G., 2004, *J. Mol. Spectrosc.*, 225, 174
- Sharpe S. W., Johnson T. J., Sams R. L., Chu P. M., Rhoderick G. C., Johnson P. A., 2004, *Appl. Spectrosc.*, 58, 1452
- Sousa-Silva C., Hesketh N., Yurchenko S. N., Hill C., Tennyson J., 2014, *J. Quant. Spectrosc. Radiat. Transf.*, 142, 66
- Sousa-Silva C., Yurchenko S. N., Tennyson J., 2013, *J. Mol. Spectrosc.*, 288, 28
- Suarez C. B., 2002, *Spectrosc. Lett.*, 35, 757
- Tarrago G., Dang-Nhu M., Goldman A., 1981, *J. Mol. Spectrosc.*, 88, 311
- Tarrago G., Lacombe N., Levy A., Guelachvili G., Bezard B., Drossart P., 1992, *J. Mol. Spectrosc.*, 154, 30
- Temma T., Baines K. H., Butler R. A. H., Brown L. R., Sagui L., Kleiner I., 2006, *J. Geophys. Res.*, 111, E12003
- Tennyson J., 2014, *J. Mol. Spectrosc.*, 296, 1
- Tennyson J., Hill C., Yurchenko S. N., 2013, in *AIP Conference Proceedings*, Vol. 1545, 6th international conference on atomic and molecular data and their applications ICAMDATA-2012, AIP, New York, pp. 186–195
- Tennyson J., Yurchenko S. N., 2012, *MNRAS*, 425, 21
- Ulenikov O. N. et al., 2002, *J. Mol. Spectrosc.*, 215, 295
- Ulenikov O. N. et al., 2004, *J. Quant. Spectrosc. Radiat. Transf.*, 83, 599
- Visscher C., Lodders K., Fegley Jr B., 2006, *ApJ*, 648, 1181

- Wang D., Shi Q., Zhu Q.-S., 2000, J. Chem. Phys., 112, 21
- Wang L., Chen P., Cheng G. S., Ding Y., Hu S. M., 2005, Spectroscopy and Spectral Analysis, 25, 1221
- Yurchenko S. N., Barber R. J., Tennyson J., 2011, MNRAS, 413, 1828
- Yurchenko S. N., Barber R. J., Yachmenev A., Thiel W., Jensen P., Tennyson J., 2009, J. Phys. Chem. A, 113, 11845
- Yurchenko S. N., Carvajal M., Jensen P., Herregodts F., Huet T. R., 2003, Chem. Phys., 290, 59
- Yurchenko S. N., Carvajal M., Thiel W., Jensen P., 2006, J. Mol. Spectrosc., 239, 71
- Yurchenko S. N., Tennyson J., 2014, MNRAS, 440, 1649
- Yurchenko S. N., Tennyson J., Bailey J., Hollis M. D. J., Tinetti G., 2014, Proc. Nat. Acad. Sci., 111, 9379
- Yurchenko S. N., Thiel W., Carvajal M., Lin H., Jensen P., 2005a, Adv. Quant. Chem., 48, 209
- Yurchenko S. N., Thiel W., Jensen P., 2007, J. Mol. Spectrosc., 245, 126
- Yurchenko S. N., Thiel W., Patchkovskii S., Jensen P., 2005b, Phys. Chem. Chem. Phys., 7, 573